Spatial control of chromosomal location in a live cell with functionalized magnetic particles

Article *in* Nanoscale · November 2015

DOI: 10.1039/c5nr04905a

4 authors, including:

Juhee Hong
Seoul National University
7 PUBLICATIONS **263** CITATIONS
SEE PROFILE

Prashant Purwar
Seoul National University
2 PUBLICATIONS **1** CITATION
SEE PROFILE

Misun Cha
Seoul National University
24 PUBLICATIONS **339** CITATIONS
SEE PROFILE

Nanoscale

PAPER

View Article Online
View Journal | View Issue

Cite this: *Nanoscale*, 2015, **7**, 19110

Spatial control of chromosomal location in a live cell with functionalized magnetic particles†

Juhee Hong,[a] Prashant Purwar,[b] Misun Cha[c] and Junghoon Lee*[a]

Received 22nd July 2015,
Accepted 17th October 2015

DOI: 10.1039/c5nr04905a

www.rsc.org/nanoscale

Long-range chromosomal travel is a phenomenon unique to cell division. Methods for non-invasive, artificial manipulation of chromosomes, such as optical or magnetic tweezers, have difficulty in producing the motion of whole chromosomes in live cells. Here, we report the spatial control of chromosomes over 10 μm in a live mouse oocyte using magnetic particles driven by an external magnetic field. Selective capture of the chromosomes was achieved using antibodies specific for histone H1 in the chromosome that were conjugated to magnetic particles (H1–BMPs). When an external magnetic field was applied, the chromosomes captured by the H1–BMPs traveled through the cytosol and accumulated near the cell membrane though the movement of the chromosomes captured by H1–BMPs was strongly disturbed by the distribution of the cytoskeleton (*e.g.* actin filaments). Being non-invasive in nature, our approach will enable new opportunities in the remote manipulation of subcellular elements.

Introduction

Cells have remarkable machinery for the efficient relocation of chromosomes, which is demonstrated in the process of cell division. During cell division, chromosomes linked to mitotic spindles are dragged through the cytosol over a long distance, comparable to the size of the cell. To date, artificial approaches have not achieved a similar long-range movement of chromosomes in a non-invasive manner. A laser-induced optical trap has been used to manipulate the location of chromosomes in a cell.[1] Despite the benefits of the optical trap, including non-invasiveness and exquisite control over positioning cellular organelles, this technique still suffers from technical challenges, such as non-specific control, limited throughput, and photo-damage.[2–4] Magnetic particles have emerged as a promising candidate for manipulating chromosomes *via* remote forces. For example, chromatin elasticity has been measured using micro magnetic beads injected directly into the nucleus.[5] In this instance, the magnetic bead was used to push the chromatin and was not intended to produce a continued motion over a long distance.

Recent progress in the reliable production and specific tailoring of functional magnetic particles has enabled a broad range of biomedical applications, such as contrast enhancement for magnetic resonance imaging (MRI), the control of cell behavior, drug delivery, and hyperthermia in cancer therapy.[6–10] Fluorescent magnetic nanoparticles in living cells were recently shown to be attracted by an external magnetic field.[11] With the possibility of remotely attracting magnetic particles, we examined the possibility of binding such particles to chromosomes and relocating the entire structure.

In this study, we used bacterial magnetic particles (BMPs) conjugated to fluorescence-labeled antibodies (H1–BMP) specifically targeting chromosomal histone H1 in mouse oocytes (Scheme 1). Histone H1 is a key protein that clamps the linker DNA wrapped around the octameric histone core, forming a nucleosome. Thus, histone H1 is an ideal targeting protein for the binding of H1–BMPs because of the abundance of histone H1 proteins in a chromosome. Careful consideration of the size and properties of the magnetic particles, which can alter the efficiency of delivery and the required magnetic force, is needed. Larger magnetic particles, such as microbeads, can exert more force from an external field but require a complex delivery mechanism such as injection, which can compromise cell viability. In contrast, smaller particles can be delivered relatively easily by endocytosis, but the amount of force they are capable of exerting from an external field is very small. For this reason, nanosized bacterial magnetic particles (BMPs: ~50 nm) produced by a magnetosome were used because of their unique characteristics, such as high magnetism, high dispersal ability in aqueous media, and good biocompatibility.[12,13] In addition, BMPs can be effectively

[a]*School of Mechanical and Aerospace Engineering, Seoul National University, 1 Gwanak-ro, Gwanak-gu, Seoul 151-744, South Korea. E-mail: jleenano@snu.ac.kr*
[b]*Division of WCU Multiscale Mechanical Design, School of Mechanical and Aerospace Engineering, Seoul National University, 1 Gwanak-ro, Gwanak-gu, Seoul 151-744, South Korea*
[c]*Department of Chemical and Biological Engineering, Korea University, 145 Anan-ro, Seongbuk-gu, Seoul, 136-713, South Korea*
†Electronic supplementary information (ESI) available. See DOI: 10.1039/c5nr04905a

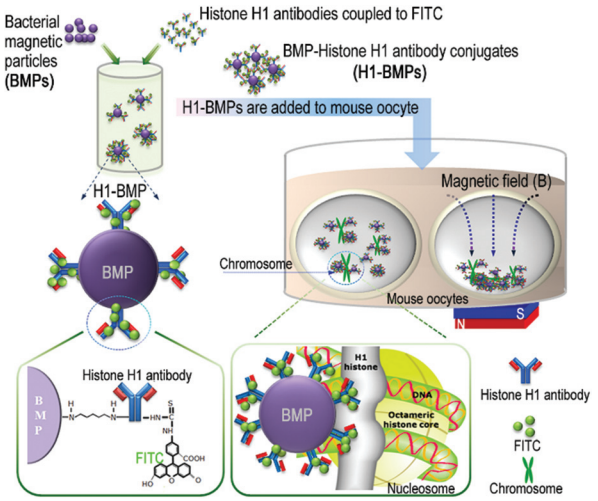

Scheme 1 Schematic illustration of spatial control of intracellular chromosomes in the live mouse oocyte by targeting histone H1 proteins in chromosomes with H1–BMPs. Antibodies to the histone H1 protein were immobilized on the BMPs for specific chromosomal targeting. After targeting the chromosomes with H1–BMPs, they were moved by applying an external magnetic field.

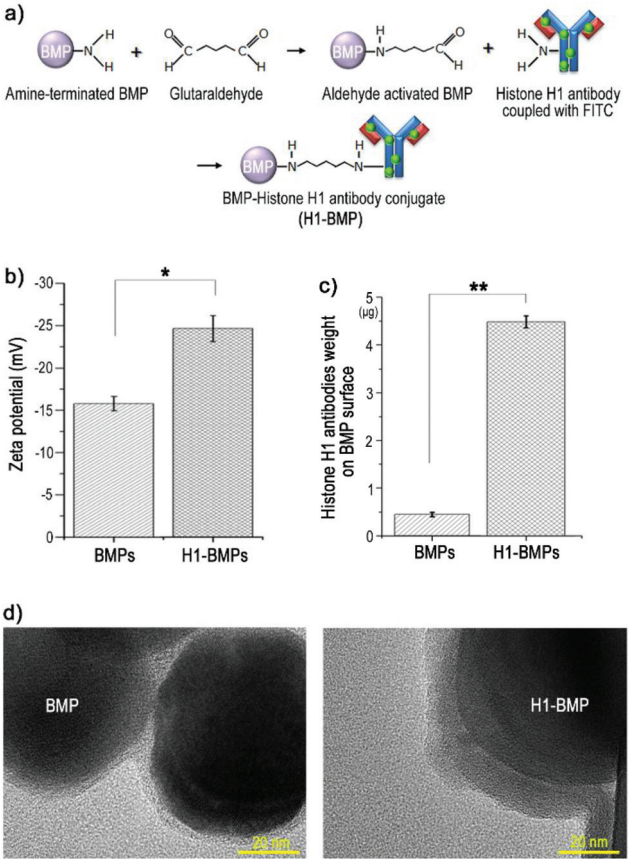

Fig. 1 H1–BMP conjugates. (a) Sequential steps of H1–BMP conjugate formation. (b) Zeta potential of BMPs and H1–BMPs. (c) Quantification of the immobilized histone H1 antibodies on the BMP surface. (d) TEM image. (Left) BMP without antibodies. (Right) BMP conjugated to antibodies (H1–BMPs). Data are expressed as mean ± standard deviations. *p and **$p < 0.05$ *versus* BMPs, ANOVA.

conjugated to diverse biomolecules due to an abundance of amine groups on particles surrounded by a lipid membrane.[14,15] To target chromosomes in a live mouse oocyte, an oocyte-specific histone antibody was used.

We first conjugated BMPs to histone H1 antibodies (H1–BMPs) and investigated whether H1–BMPs have a specific affinity to chromosomes. Based on this result, cell orientation was controlled by applying an external magnetic field and an experiment of chromosome manipulation was carried out.

Our approach will provide new opportunities for investigating the cellular functions associated with the spatio-temporal distribution of such components.

Results and discussion

Characteristics of H1–BMPs

The size distribution of the collected bacterial magnetic particles (BMPs) ranges from 30 to 70 nm in diameter. The mean diameter of BMPs was about 49.6 ± 2.3 nm (Fig. S1†). To target the histone H1 protein in chromosomes, oocyte-specific histone H1 antibodies (32 kDa, ab71580, Abcam, USA) were used. The covalent binding of histone H1 antibodies to the amine-terminated BMP surface was carried out with glutaraldehyde as shown in Fig. 1a. After conjugation of H1–BMPs, the excess unbound antibodies were removed using a magnetic bar (Fig. S2†). Whether the antibodies were immobilized on the BMP surface was investigated by using zeta potential analysis, BCA assay, and TEM.

First the change of BMP surface charge was investigated before and after immobilization of the antibody. As depicted in Fig. 1b, the surface charges of BMPs and H1–BMPs were measured as −15.79 mV and −24.64 mV, respectively. The BMP surface charge is composed of the positive charge of the amine group and the negative charge of the lipid membrane. Thus, the immobilization process decreases the positive charge by blocking the amine group on the BMP membrane, leading to an increase of negative charge in the H1–BMP surface when the antibodies were immobilized.

Second, we measured the concentration of antibodies on the BMP surface by using the bicinchoninic acid (BCA) assay (Fig. 1c). Prior to the measurement of the antibody weight on the H1–BMP surface, the BMP sample was pre-measured since it already has some proteins.[16] 6 μg antibodies were used for conjugation. H1–BMPs (weight 43.75 μg) had 4.48 μg proteins on their surface compared to 0.42 μg proteins on the unconjugated BMPs' surface. Thus, the loading efficiency is calculated as ~68%. Through this result, the average number of antibodies on the BMP surface was theoretically calculated as ~550 antibodies (packing density ≈ 1).

Lastly, the histone H1 antibodies on the BMP surface were directly observed using transmission electron microscopy (TEM). While the membrane of BMP has a thickness of

4–5 nm, the size of the H1–BMP membrane is around 12–13 nm as shown in Fig. 1d. This difference may be due to the immobilization of the histone H1 antibodies on the BMP surface.

Analysis of magnetic force

As a first step towards the spatial control of chromosomes, the amount of the applied magnetic force was analyzed. Prior to calculation, the applied magnetic field was measured (Fig. S3†). To generate a strong magnetic field, several neodymium magnets were used depending on the experimental conditions. Assuming the BMP as a point like magnetic dipole, we can calculate the magnetic force on a single BMP under an external magnetic field gradient as follows. The magnetic force F_m on a point like magnetic dipole m in a magnetic field B can be calculated as[17,18]

$$F_m = (m\cdot\nabla)B$$

If the volume of a particle is V_m and the effective susceptibility relative to the surrounding medium (here the cytoplasm) is $\Delta\chi$

$$F_m = \frac{V_m\Delta\chi}{\mu_0}(B\cdot\nabla)B$$

where μ_0 is the magnetic permeability of vacuum. According to the Maxwell equation in a time invariant magnetic field $\nabla\times B = 0$, so the above equation can be written as

$$F_m = V_m\Delta\chi(\nabla|B^2|/2\mu_0)$$

If the cytoplasm effective susceptibility is assumed to be equivalent to that of water, it can be neglected compared to the BMP volumetric direct current (DC) susceptibility.[19]

We calculated the magnetic forces based on the measurement of the magnetic field in two different cases as shown in Fig. 2. In the control of cell rotation, we applied 30 mT magnetic field which generated a magnetic force of ~50 fN on a single BMP using a combination of small magnets. In addition, in the control of chromosome location, a permanent neodymium magnet (50 mm × 50 mm × 25 mm) was used at 1.5 mm from oocytes. The measured magnetic field at a distance of 1.5 mm was ~500 mT which resulted in a force of ~780 fN on a single BMP. On the other hand, in time course monitoring of chromosomal movement using a microfluidic cell trapping device, a combination of small magnets was used at a distance of 5 mm because of the space limitation in the device. The measured magnetic field at a distance of 5 mm was ~170 mT which resulted in a force of ~230 fN on single BMPs.

It was calculated that a large sub-piconewton force (~800 fN) was exerted on a single BMP by an external magnetic field ($|B| \cong 500$ T m^{-1} at 1.5 mm).

Based on the calculation, it is estimated that the approximate magnetic force exerted on chromosomes (ESI section 1†) would be sufficient to drag chromosomes (several tens of piconewtons).[20,21]

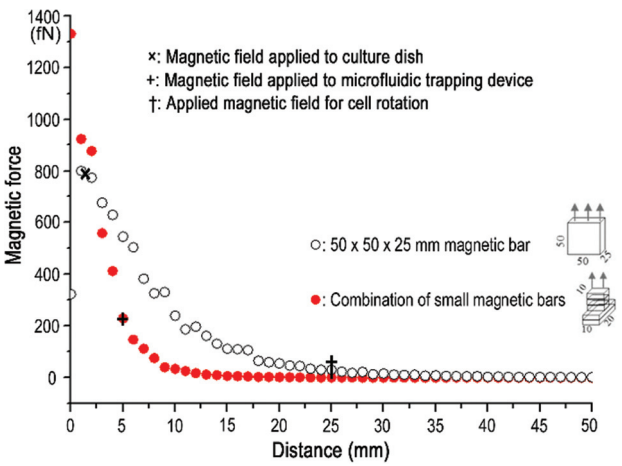

Fig. 2 Analysis of the magnetic force on a single BMP. Dimensions are in mm.

Specific targeting of chromosomes in a live oocyte

We investigated whether H1–BMPs have specific affinity to the chromosomal histone H1 protein in oocytes. Oocytes were collected from C57BL/6 female mice. In these experiments, immature oocytes at the germinal vesicle breakdown (GVBD) stage were selected for subsequent experiments because the nuclear envelope can significantly hinder the free passage of H1–BMPs into the nucleus for chromosomal targeting (Fig. S4†). Furthermore, the immature oocyte facilitates the monitoring and analysis of chromosomal movement in contrast to the mature oocyte, as chromosomes in the mature oocyte (metaphase II) are already located near the cell membrane.[22]

The confocal images of oocytes show the specific targeting of H1–BMPs to histone H1 on chromosomes. In case 1 (Fig. 3a), "without antibodies," the FITC spots (green) were randomly scattered inside the oocyte and showed no correlation with chromosomal distribution (blue). In case 2 (Fig. 3b), "with antibodies," most of the FITC spots co-localized with the DAPI-stained chromosomes. This observation indicates that the internalized H1–BMPs were well guided and specifically targeted to the chromosomes, despite the highly crowded cytosol and other subcellular structures.[23,24]

Control of cell orientation

Based on the specific targeting test, we attempted to rotate the cell using a remote magnetic field as shown in Fig. 4. A magnetic field was applied to stationary cells at a specific distance ($|B| \cong 30$ mT at 25 mm) using a neodymium magnet to avoid oocyte's translational motion when a magnetic field approaches the oocyte. The extracellular H1–BMPs were removed by several pipetting after the chromosomes had already been targeted with H1–BMPs. To apply the maximum torque for cell rotation, we selected an oocyte with all of the chromosomes focused at the cortex. When the magnet was slowly moved from the top of the cell to the bottom and

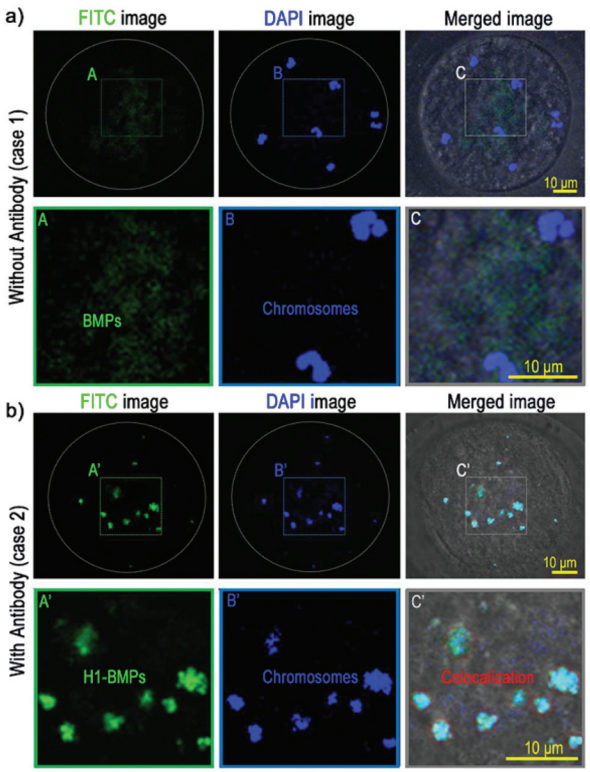

Fig. 3 (a) Specific targeting of BMPs without antibodies (BMP–FITC conjugates) to chromosomes inside a live oocyte. (b) BMPs with antibodies (H1–BMPs).

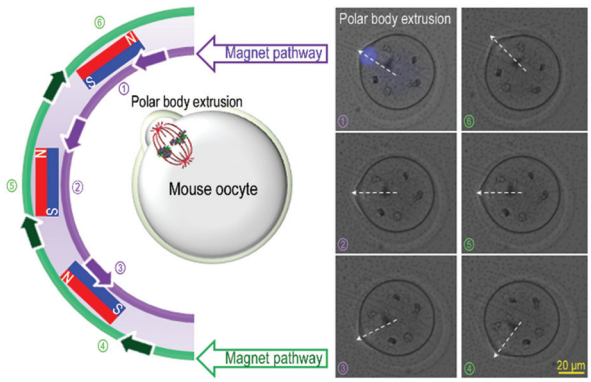

Fig. 4 Rotation of the cell by an external magnetic field. The blue spot in image ① is the Hoechst-stained location of the chromosome.

vice versa for 8–10 seconds, the cell rotated, following the path of the magnetic bar (ESI Movie S1†). The oocyte rotation may contribute to the internal motion of the chromosomes because the H1–BMPs were concentrated near the membrane and the oocyte was not anchored.

Control of chromosome location in a live oocyte

Next, we attempted to move the chromosomes that are normally localized to the center of a live oocyte using the

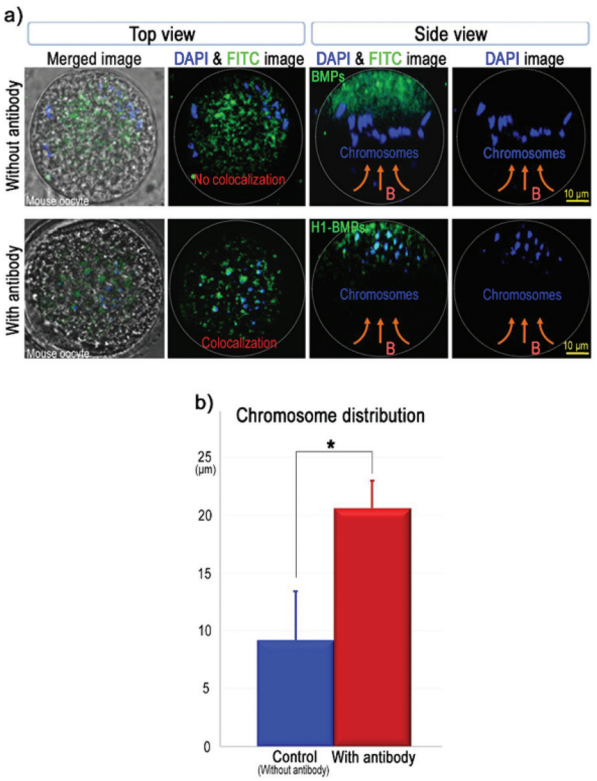

Fig. 5 Spatial control of the targeted chromosomes with H1–BMPs in a live oocyte. (a) Experimental results of chromosome repositioning using H1–BMPs. Confocal microscopy images were processed and re-oriented to align the *z*-axis in the direction of the highest BMP concentration from the center. (b) Quantitative analysis of chromosomal distribution (n = 5 each). Data are expressed as the mean ± standard deviation. *p < 0.05 compared to control by ANOVA.

H1–BMPs. To observe maximum chromosome movement by H1–BMPs, a strong magnetic field ($|B| \cong 500$ mT at 1.5 mm) was applied using a magnetic bar placed directly under the culture dish for 12 h (Fig. S5† for Experimental details). Then, confocal images were obtained after cell fixation and chromosome staining with 4′,6-diamidino-2-phenylindole (DAPI) and reconstructed to localize the fluorescent spots using Image J software. Fig. 5a shows the experimental results. Without antibodies, the BMPs did not conjugate to the chromosomes, and the chromosomes did not move together with the BMPs in the presence of the magnetic field (Fig. 5a, upper image). The green spots from the FITC-conjugated BMPs moved in the direction of the magnetic field, whereas the blue spots from the DAPI-stained chromosomes remained close to the center. With the antibody, the blue spots (chromosomes) coincided with the green spots (H1–BMPs), which noticeably moved toward the top (Fig. 5a, lower image).

For a more detailed analysis, chromosomal movement was quantitatively assessed by image processing. The mass center of the blue signal was calculated and used as a value representing the entire distance moved. The distances with and without antibodies were compared. A substantial difference is observed

between the cases with (20.59 ± 2.47 μm) and without (9.18 ± 4.23 μm) antibodies as shown in Fig. 5b. It is obvious that this difference in chromosomal movement is caused by an external magnetic field rather than cytoplasmic reorganization such as cytoplasmic F-actin. Considering the oocyte radius, it is found that chromosomes were largely moved by an external magnetic field. However, chromosomes did not move up to the cell membrane despite the application of a magnetic field for 12 h. It is expected that there will be obstacles to chromosome movement inside oocytes such as F-actin filaments.

Time course of monitoring chromosome movement

To gain further evidence of chromosomal movement by a remote magnetic field, we observed the time course of chromosome motion in a live oocyte. To observe the lateral movement, we prevented the rotation and drift of the living oocyte by anchoring it to the substrate. For this purpose, we designed and developed a vacuum-assisted microfluidic device to trap the oocyte on a transparent substrate as shown in Fig. 6a and b.

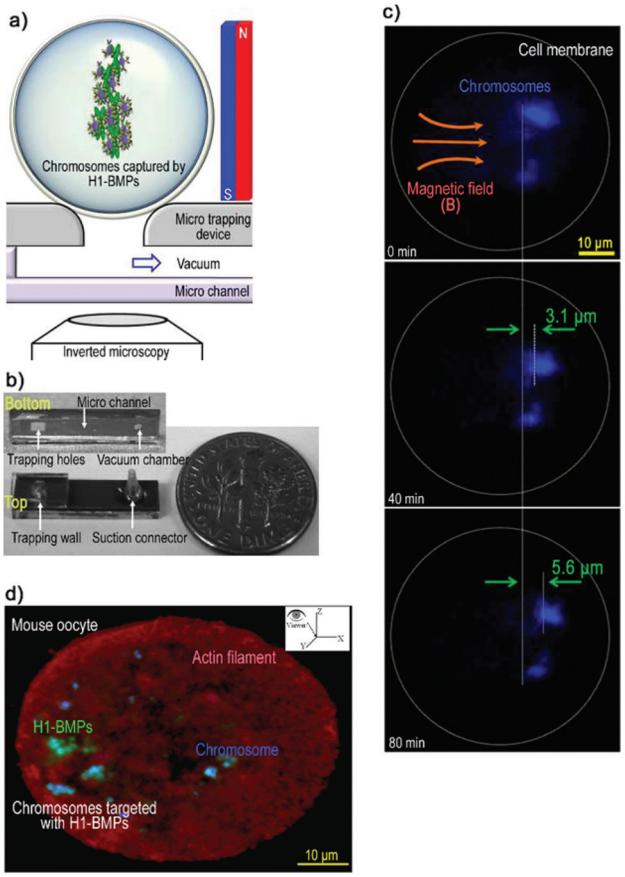

Fig. 6 Time course of monitoring chromosome movement. (a) Schematic diagram of a vacuum-assisted microfluidic cell device. (b) A fabricated vacuum-assisted microfluidic cell trapping device. (c) Experimental results of the time course of chromosomal movement. (d) Tilted view of the oocyte produced by reconstructing the confocal images (actin filament: red, H1–BMPs: green, chromosomes: blue, light blue: overlapping of green and blue).

A microfluidic device was fabricated integrating the cell trapping part and the microchannel part (Fig. S6†). The fabricated device was tested using ~80 μm micro polybeads (ESI Movie S2†). The live oocytes were Hoechst-stained before being immobilized on the trapping hole (Fig. S6†). When a negative pressure was applied to the microfluidic device, the oocytes were rapidly attracted to and fixed on the holes. A magnetic field was applied to the side of the trapped oocyte ($|B| \cong$ 170 mT at 5 mm), and the images were captured by inverted microscopy at 10 min intervals for 80 min to avoid photobleaching. The sequence of captured images shows the lateral motion of chromosomes toward the applied magnetic field in the live oocyte as depicted in Fig. 6c (ESI Movie S3†). The velocity of chromosomal movement induced by the remote magnetic force was calculated to be ~70 nm min^{-1} over an average distance of 5.6 μm. The chromosomes targeted with H1-BMPs were moved toward the direction of an external magnetic field, despite obstacles inside oocyte such as entanglement resistance of actin filaments, as shown in Fig. 6d.

It is shown that the actin filament density is high at the cell periphery, known as the cell cortex. Thus, it was expected that chromosomes at the cell cortex will be strongly affected by the actin filament meshwork compared to the chromosomes located at the center of the cell where the chromosomal movement was initiated. Thus, chromosomes did not move up to the cortex due to the high density of the actin filament at the cortex.

Conclusions

Artificial control of chromosome movement is a difficult challenge for manipulating the motion of whole chromosomes in live cells. In this study, we demonstrate non-invasive, artificial chromosomal motion by the targeting of chromosomal histone H1 proteins in a live mouse immature oocyte. To this end, we used bacterial magnetic particles (BMPs) to conjugate to histone H1 antibodies (H1–BMPs). H1–BMPs have a specific affinity to the chromosomal histone H1 protein. After targeting chromosomes with H1–BMPs, spatial control of chromosome location was manipulated by applying an external magnetic field. The chromosomes moved to over 10 μm from the cell center. Novel procedures and techniques for efficient delivery and tracking were developed.

Our approach will provide new opportunities for cellular research that requires the relocation of chromosomes by remote forces. Our method, if extended to remotely control the locations of other subcellular components, could also provide a useful tool for investigating the cellular functions associated with the spatiotemporal distribution of such components.

Experimental details

Preparation of bacterial magnetic particles (BMPs)

Bacterial magnetic nanoparticles (BMPs) were obtained from *Magnetospirillum magneticum* sp. AMB-1 which was cultured in

magnetic spirillum growth medium (MSGM) for 4–5 days at 27 °C under anaerobic conditions (Biofree incubator, Korea). Cultured *Magnetospirillum* sp. AMB-1 was centrifuged for 25 min at 11 300*g* and then lysed by sonication (VCX500, Sonics & Materials, USA) for 30 min. The BMPs were collected using a neodymium iron boron (NdFeB) magnet, then washed 5 times with 1× phosphate-buffered saline (PBS), and finally dispersed in 1× PBS. The collected BMPs were sterilized by autoclaving (121 °C, 15 min). The concentration of BMPs was measured by inductively coupled plasma mass spectrometry (ICP, Shimadzu, Japan).

Bacterial magnetic particles (BMPs)–histone H1 antibody conjugates (H1–BMPs)

For covalent coupling of amine-terminated BMP and oocyte-specific histone H1 antibodies (~32 kDa, ab71580, Abcam, USA), the surface of the BMPs was pretreated with a 10% glutaraldehyde solution (Sigma, USA) as the crosslinking agent.[25] After the reaction for 1–2 h at room temperature with continuous mixing, the BMPs were washed twice with 1 ml of 2-(*N*-morpholino)ethanesulfonic acid (MES buffer, Sigma, USA). Prior to the immobilization of antibodies on the BMP surface, histone H1 antibodies (immunoglobulin G: IgG) were labeled with fluorescein isothiocyanate (FITC) by using the EZ-Label FITC Protein Labeling Kit (Thermo Scientific, USA). 12.48 μl FITC solution was completely mixed in 100 μl dimethylformamide (DMF) solution, and then the mixture of FITC and DMF was added to a 20 μl solution of antibodies. After incubating at room temperature for 1 h, the dialysis process was used to remove the uncoupled FITC. Based on the theoretical calculation of the average number of antibodies on the nanoparticle surface,[26] the resuspended ~146 μg BMPs in MES solution (0.1×) were added to the reaction tube containing the histone H1 antibodies coupled with FITC. The mixture was reacted for 2–4 h with continuous mixing. The BMPs conjugated with the histone H1 antibodies (H1–BMPs) were concentrated by using a magnetic bar to remove the excess of unbound antibodies and washed several times with MES buffer. Then, the H1–BMPs were stored in buffer solution (0.3% bovine serum albumin (BSA) in 1× PBS). The concentration of H1–BMPs was measured by inductively coupled plasma mass spectrometry (ICP, Shimadzu, Japan).

Characteristics of H1–BMPs

We investigated the characteristics of H1–BMP whether the antibodies were well immobilized on the BMP surface.

First, the concentration of nanoparticle-attached proteins was estimated using the bicinchoninic acid (BCA) protein assay kit (Thermo Scientific, USA). A convenient standard curve can be drawn using bovine serum albumin (BSA) with concentrations of 0, 25, 125, 250, 500, 750, 1000, 1500, and 2000 μg mL^{-1} for the standard assay. The concentration of antibodies was measured in triplicate for each sample. As a first step towards the measurement of the immobilized histone H1 antibodies on the BMP surface, the existing proteins on BMPs were measured as a control experiment. 200 μl working reagent was mixed with 25 μl of dispersed nanoparticles (BMP and H1–BMP concentration: 1.75 μg μl^{-1}) by shaking at 37 °C. After reaction for 30 min, the absorbance was measured at 571 nm using a microplate reader (Thermo Scientific, USA). Prior to the measurement, the BMPs in the sample were removed in order to prevent the absorbance disturbance. The amount of protein was calculated from a standard curve.

Next, to investigate the change of surface charge before and after immobilization of the antibodies on the BMP surface, the zeta potential of BMPs and H1–BMPs was determined by using an electrophoretic light scattering spectrophotometer (ELS-8000, Otsuka Electronics, Japan).

Lastly, we observed immobilization of histone H1 antibodies on the BMP surface using a high resolution transmission electron microscope (HRTEM, JEM-ARM200F, Japan) operating at 80 kV. Prior to observation by HRTEM, both the samples were stained negatively using phosphotungstic acid (PTA, 2%) after the suspended samples were deposited onto a carbon coated copper grid (200 mesh).

Collected immature oocytes and prepared samples

Animal care and handling were conducted in accordance with the policy and regulation for the care and use of laboratory animals at Seoul National University (SNU-101214-1 and SNU-130808-1-2). Six-week-old C57BL/6 female mice were superovulated with the injection of 5 IU ml^{-1} Pregnant Mare Serum Gonadotropin (PMSG, Folligon, Intervet International, Boxmeer, Netherlands) and 5 IU ml^{-1} human Chorionic Gonadotropin (hCG, Pregnyl, Organon, Oss, the Netherlands) and were administered 48 h post-PMSG injection. Subsequently, the cumulus-oocyte-complex (COC) was retrieved from the oviduct 17 h post-hCG injection. The cumulus cells of COC retrieved from a mouse ovary were enzymatically removed by treating with 200 μl hyaluronidase solution (80 IU mL^{-1}, Irvine Scientific, USA) for 1 min. The oocytes were pipetted in and out through a fine-bore glass pipette to loosen the weakened cumulus mass, and then transferred to fresh M16 medium (Sigma, USA).

For cell cycle arrest which can prevent the spontaneous chromosome movement during the experiment, 0.3 μM nocodazole treatment (Sigma Aldrich, USA) in dimethylsulfoxide solution (DMSO, Sigma, USA) was carried out. The nocodazole was diluted in M16 medium to yield a final concentration of 2.1 nM.

Delivery of H1–BMPs into oocyte

After nocodazole treatment, H1–BMPs with a final concentration of 1 μg ml^{-1} were added in culture medium and a weak magnetic field was applied at the bottom of the culture dish to increase cellular uptake.[27] The H1–BMPs remaining outside the cells were removed by pipetting after 16–18 h. Then, immature oocytes at the germinal vesicle breakdown (GVBD) stage were selected for subsequent experiments. Confocal laser scanning microscopy (CLSM, Zeiss, USA) was used to obtain images.

Measurement of the magnetic field

We used a neodymium magnet to generate a strong magnetic field. Neodymium magnets of various sizes were placed at different distances from the sample, depending on experiments. The magnetic field *vs.* distance was measured from the surface of a magnet at an interval of 1 mm using a Tesla meter (Kanetec, Japan).

Analysis of chromosome distribution inside the oocyte

The analysis of chromosome distribution in the oocyte was performed by using the Matlab software (Mathworks, USA). Chromosomal blue spots were segmented out through image processing, from confocal microscopy images. The mass center of blue spots of each slide was calculated. To find the center of mass as a whole, all individual slides' mass center was averaged out considering the no. of chromosomal pixels on each slide and then the distance of this mass center from the center of oocyte was calculated.

Vacuum-assisted microfluidic cell trapping device

In order to achieve the time course monitoring of chromosomes, it was crucial to prevent the rotation of the cell by anchoring to the substrate. For the anchoring purpose, we fabricated a vacuum-assisted microfluidic cell trapping device using a silicon-on-glass (SOG) wafer and transparent polydimethylsiloxane (PDMS, Dow Corning, USA). First, the trapping device was fabricated by two etching processes such as 400 μm thick Si and 30 μm thick glass using deep-reactive ion etching (DRIE). Aluminum was used as the mask for the deep reactive ion etching (DRIE) process. After etching the glass by DRIE, the aluminum layer was removed. Next, the microchannel was fabricated *via* a PDMS replication process. A mold was created with SU-8, spin-coated and patterned. The PDMS mixture (curing agent : PDMS = 1 : 10) was placed in a vacuum chamber for 1 h to remove the trapped gases, and then poured onto the mold. After PDMS curing, the separate parts were assembled into the final microfluidic trapping device using a biocompatible UV epoxy. The oocytes in the medium chamber were trapped at the holes, which were connected to the vacuum chamber. Considering the size of the oocytes, the holes of various sizes between 20–50 μm were designed to find the optimal capturing conditions. The chamber pressure was controlled by using a micromanipulator (IM-9B and 9C, Narishige, Japan), which was attached to an inverted microscope (TE 2000-E, Nikon, Japan). To monitor the dynamic chromosome movement, a portable incubator (IC-L-10, Chamlide, Korea) which can maintain constant temperature, humidity, and CO_2 was used.

Fluorescence staining

Actin filaments were stained with TRITC-conjugated phalloidin (Millipore, USA). Prior to actin filament staining, 15 μg TRITC-conjugated phalloidin was dissolved in 250 μl methanol. The fixed oocytes were permeabilized with 0.1% Triton X-100 in 1× PBS for 10 min at room temperature and washed three times with PBS. To block nonspecific binding, a blocking solution (1% bovine serum albumin (BSA) solution in 1× PBS) was added over 30 min and the oocytes were washed three times with 1× PBS. To stain actin filaments, oocytes in 1 ml medium were stained with 2 μl TRITC-conjugated phalloidin (dilution ratio = 1 : 500) and incubated for 30 min at room temperature in the dark. After washing three times, the oocytes were labeled with 4′,6-diamidino-2-phenylindole (DAPI, Millipore, USA) or Hoechst (Millipore, USA) over 10 min (dilution ratio = 1 : 1000) depending on experiments.

Confocal laser scanning microscopy (CLSM)

Confocal laser scanning microscopy (CLSM) is an invaluable tool for a wide range of investigations in biological and medical sciences because of high-resolution optical images with a depth selectivity ranging in thickness up to 100 micrometers. The key feature of confocal laser scanning microscopy is its ability to collect in-focus images from selected depths, a process known as optical sectioning. These sectioning images enable us to reconstruct a 3D image of a complex object.

Statistical analysis

Data were expressed as mean standard deviation. Statistical analysis was carried out using statistical software (SAS 9.4, USA). Differences were considered significant when $P < 0.05$.

Acknowledgements

This work was supported by the Center for Integrated Smart Sensors funded by the Ministry of Science, ICT & Future Planning as Global Frontier Project (CISS-2011-0031866). This research was also supported by a grant to the Bio-Mimetic Robot Research Center funded by Defense Acquisition Program Administration, and by the Agency for Defense Development (UD130070ID). The fabrication was performed at the Interuniversity Semi-conductor Research Center (ISRC) in Seoul National University. The authors thank S. Lee for fruitful discussions, and J. Y. Kang for suggestions for experiments. The authors also thank T. H. Park for supporting the bacterial magnetic particles (BMPs).

Notes and references

1 M. W. Berns, W. H. Wright, B. J. Tromberg, G. A. Profeta, J. J. Andrews and R. J. Walter, *Proc. Natl. Acad. Sci. U. S. A.*, 1989, **86**, 4539–4543.
2 K. Konig, H. Liang, M. W. Berns and B. J. Tromberg, *Nature*, 1995, **377**, 20–21.
3 C. Bustamante, J. C. Macosko and G. J. Wuite, *Nat. Rev. Mol. Cell Biol.*, 2000, **1**, 130–136.
4 K. C. Neuman and A. Nagy, *Nat. Methods*, 2008, **5**, 491–505.
5 A. H. de Vries, B. E. Krenn, R. van Driel, V. Subramaniam and J. S. Kanger, *Nano Lett.*, 2007, **7**, 1424–1427.

6 O. T. Bruns, H. Ittrich, K. Peldschus, M. G. Kaul, U. I. Tromsdorf, J. Lauterwasser, M. S. Nikolic, B. Mollwitz, M. Merkel, N. C. Bigall, S. Sapra, R. Reimer, H. Hohenberg, H. Weller, A. Eychmuller, G. Adam, U. Beisiegel and J. Heeren, *Nat. Nanotechnol.*, 2009, **4**, 193–201.
7 J. Dobson, *Nat. Nanotechnol.*, 2008, **3**, 139–143.
8 M. Arruebo, R. Fernández-Pacheco, M. R. Ibarra and J. Santamaría, *Nano Today*, 2007, **2**, 22–32.
9 M. Ferrari, *Nat. Rev. Cancer*, 2005, **5**, 161–171.
10 H. Rudolf, D. Silvio, M. Robert and Z. Matthias, *J. Phys.: Condens. Matter*, 2006, **18**, S2919.
11 J. Gao, W. Zhang, P. Huang, B. Zhang, X. Zhang and B. Xu, *J. Am. Chem. Soc.*, 2008, **130**, 3710–3711.
12 R. P. Blakemore, *Annu. Rev. Microbiol.*, 1982, **36**, 217–238.
13 S. Mann, R. B. Frankel and R. P. Blakemore, *Nature*, 1984, **310**, 405–407.
14 Y. A. Gorby, T. J. Beveridge and R. P. Blakemore, *J. Bacteriol.*, 1988, **170**, 834–841.
15 J. Xie, K. Chen and X. Chen, *Nano Res.*, 2009, **2**, 261–278.
16 A. S. Fabritius, M. L. Ellefson and F. J. McNally, *Curr. Opin. Cell Biol.*, 2011, **23**, 78–84.
17 T. H. Boyer, *Am. J. Phys.*, 1988, **56**, 688–692.
18 Q. A. Pankhurst, J. Connolly, S. K. Jones and J. Dobson, *J. Phys. D: Appl. Phys.*, 2003, **36**, R167.
19 R. Hergt, R. Hiergeist, M. Zeisberger, D. Schüler, U. Heyen, I. Hilger and W. A. Kaiser, *J. Magn. Magn. Mater.*, 2005, **293**, 80–86.
20 G. Bao and S. Suresh, *Nat. Mater.*, 2003, **2**, 715–725.
21 F. M. Fazal and S. M. Block, *Nat. Photonics*, 2011, **5**, 318–321.
22 S. Brunet and B. Maro, *Reproduction*, 2005, **130**, 801–811.
23 K. Luby-Phelps, *Int. Rev. Cytol.*, 2000, **192**, 189–221.
24 Z. Holubcová, G. Howard and M. Schuh, *Nat. Cell Biol.*, 2013, **15**, 937–947.
25 M. Arruebo, R. Fernández-Pacheco, B. Velasco, C. Marquina, J. Arbiol, S. Irusta, M. R. Ibarra and J. Santamaría, *Adv. Funct. Mater.*, 2007, **17**, 1473–1479.
26 L. L. Ma, J. O. Tam, B. W. Willsey, D. Rigdon, R. Ramesh, K. Sokolov and K. P. Johnston, *Langmuir*, 2011, **27**, 7681–7690.
27 F. Scherer, M. Anton, U. Schillinger, J. Henke, C. Bergemann, A. Kruger, B. Gansbacher and C. Plank, *Gene Ther.*, 2002, **9**, 102–109.